CrossMark

High-resolution imaging of the nanostructured surface of polyacrylonitrile-based fibers

Christina Kunzmann[1,*] (iD), Judith Moosburger-Will[2], and Siegfried Horn[1,2]

[1] *Experimental Physics II, Institute of Physics, University of Augsburg, 86135 Augsburg, Germany*
[2] *Institute of Materials Resource Management, University of Augsburg, 86135 Augsburg, Germany*

ABSTRACT

In our study, we present atomic force microscopy (AFM) investigations of the surface of Polyacrylonitrile-based carbon fibers utilizing two different AFM probes, a standard tip as used in literature up to now and a recently made available super sharp tip. Using the super sharp tip, we identified so far not reported pore-like nanostructures distributed homogeneously over the surface of the fibers. We show that such nanopores are already present on the surface of the corresponding precursor fiber, indicating that these structures are characteristic for the fiber along the production process. To investigate a possible correlation between the surface structures and the mechanical properties of carbon fibers, we further analyzed the surface of various carbon fibers showing different tensile strengths. All investigated fibers show characteristic nanoporous surface structures and a correlation was found between the Nanopore size and shape and the mechanical properties. The effective nanopore area and the aspect ratio of the nanopores decrease with increasing tensile strength of the fibers. In addition, the nanoroughness of the fiber surface is correlated to the nanopore size and also decreases with increasing tensile strength.

Introduction

Due to the increasing spread of carbon fiber-reinforced composite materials in aerospace, automotive and, more recently, manufacturing systems engineering, the demand for carbon fibers is continuously growing [1–4]. The need to improve the production process and the properties of the carbon fibers has promoted increasing research efforts over the last decades. As a result, commercial carbon fibers are available with different tensile strengths, moduli, or strains [5]. The

most important precursor material for carbon fiber production is polyacrylonitrile (PAN), which is prevalently used due to the high tensile strength of the resulting carbon fibers and the acceptable cost of production [6, 7]. PAN fibers are produced by a wet spinning process, in which a PAN/solvent solution is spun into a liquid coagulation bath [7–13]. After immersion in the nonsolvent coagulation bath, the solution becomes thermodynamically unstable and spinodal decomposition in two phases occurs—a process generally typical for polymer solutions

Address correspondence to E-mail: christina.kunzmann@physik.uni-augsburg.de

[9–11, 14]. A polymer-rich phase forms the bulk of the fiber, while a solvent-rich phase forms voids [9–11]. This structure is called gel network [14]. It was shown that the shell of such fibers is porous and the pore size depends on the conditions of the coagulation [11, 13, 15]. After coagulation, the fibers undergo repeated steps of washing and stretching. Here, the polymer molecules become orientated, which determines the properties of the PAN fiber [16]. Finally, a textile finish is applied to protect the fibers and to ease their handling in the following steps of stabilization and carbonization [8]. The quality of the carbon fibers is closely linked to the properties of the PAN precursor and it takes comprehensive knowledge of the precursor fiber chemistry and microstructure to improve the properties of the carbon fibers [17–19]. In particular, the surface structure of the fiber is in focus of research, since it is assumed to be correlated to fiber properties and the fiber–matrix interaction, e.g., by mechanical interlocking [20, 21].

The microstructure of PAN and PAN-based carbon fibers has been studied by X-ray diffraction (XRD) [22, 23], scanning electron, and transmission electron microscopy (SEM and TEM) [24–28]. Scanning tunneling and atomic force microscopy (STM and AFM) have been used to investigate the fiber surface [20, 29–37]. Magonov et al. [37] and Li et al. [36], using SEM and STM, found grain-type features on the carbon fiber surface and presented a structural model of high modulus and high-strength carbon fibers based on these granules [36]. It should be noted, however, that STM images present a superposition of topographic and electronic information. Further, the STM technique cannot be applied to nonconducting polymer precursor fibers and fibers after the intermediate stabilization steps. In contrast, the AFM technique allows to investigate directly the surface topography of carbon fibers as well as nonconducting fibers [35, 38]. AFM permits a nondestructive characterization of the surface morphology and allows collection of

Figure 1 AFM height and phase images of a carbon fiber surface (CF HS) scanned with TESPA probe (**a**, **b**) and with EBD-SSS probe (**c**, **d**).
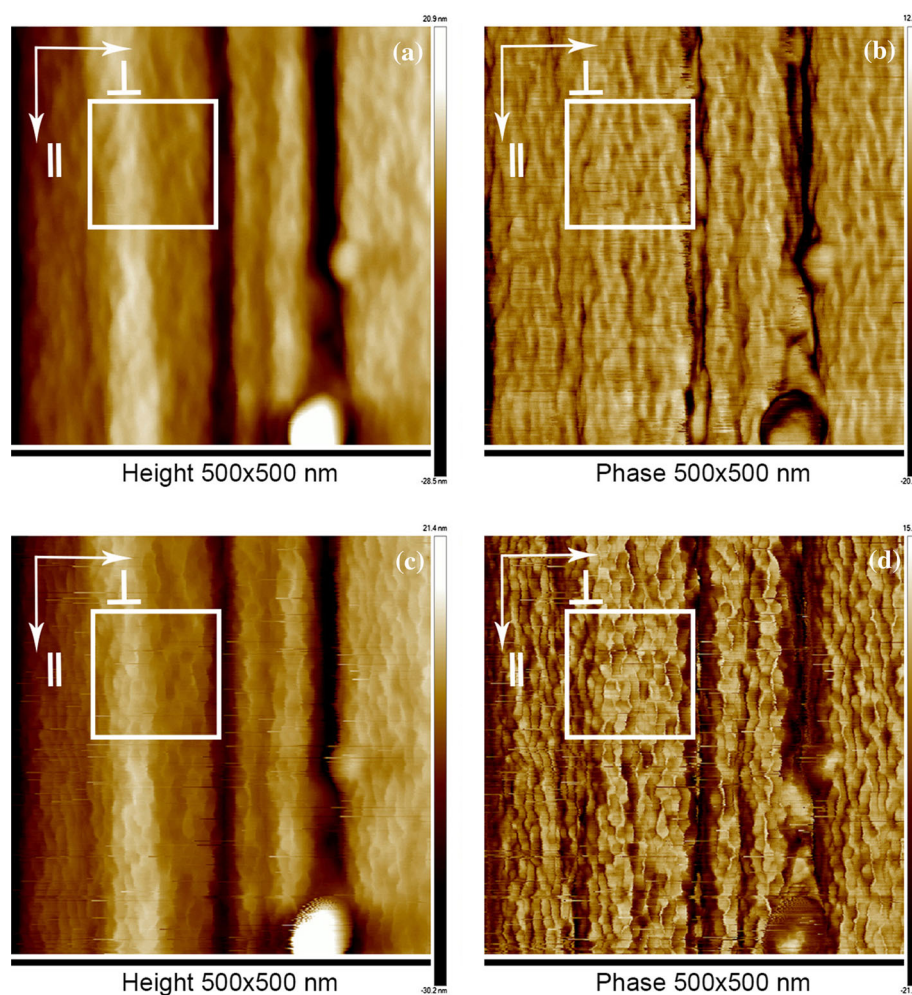
quantitative lateral and height information on nanoscale [39, 40]. The lateral resolution depends sensitively on the geometry and durability of the tip used [41–43]. In recent years, newly developed technologies allow the production of tips with high aspect ratio and small diameter [44]. Such tips allow precise measurements of nanoscale structures.

Here, we present an investigation of the surface structures of PAN-based carbon fibers using the AFM in tapping mode with both, a standard tip and a recently made available super sharp tip. Using such a super sharp tip, we find a nanoporous structure on all fibers investigated, in particular on both carbon as well as PAN precursor fibers. A possible correlation between the nanoscale surface structure of carbon fibers and their mechanical properties is proposed.

Experimental

In this study, we analyzed untreated (surface not activated, unsized) high-tensile strength PAN-based carbon fibers (CF HS) and the corresponding precursor fibers (PAN), equipped with a textile finish. We further investigated the surface of high tensile strength (T700S, T300) and high modulus/low tensile strength (M40) Toray carbon fibers, originally equipped with an epoxy-based sizing [45–47]. To analyze the surface of the respective fibers on a nanoscale finish and sizing of the fibers were removed. To this end, the finish of the PAN fibers was solved in 0.1 M/L solution of Tetrabutylammonium fluoride trihydrate (TBAF, ACROS Organics, 90 %) in Tetrahydrofuran (THF, Sigma Aldrich, ≥99.9 %), while the carbon fibers were desized by a thermal treatment at 800 °C under Argon atmosphere.

The AFM measurements of the fibers were performed using a Bruker Dimension ICON in tapping mode both with standard TESPA probes from Bruker (tip radius 8 nm) and super sharp EBD-SSS NCHR AFM probes from Nanotools (tip radius 2–3 nm) showing a higher aspect ratio compared to standard tips. Both AFM height and phase images were recorded. The scanning area of the images was 500 nm × 500 nm (512 × 512 pixels); the scanning area of high magnification images was reduced to a
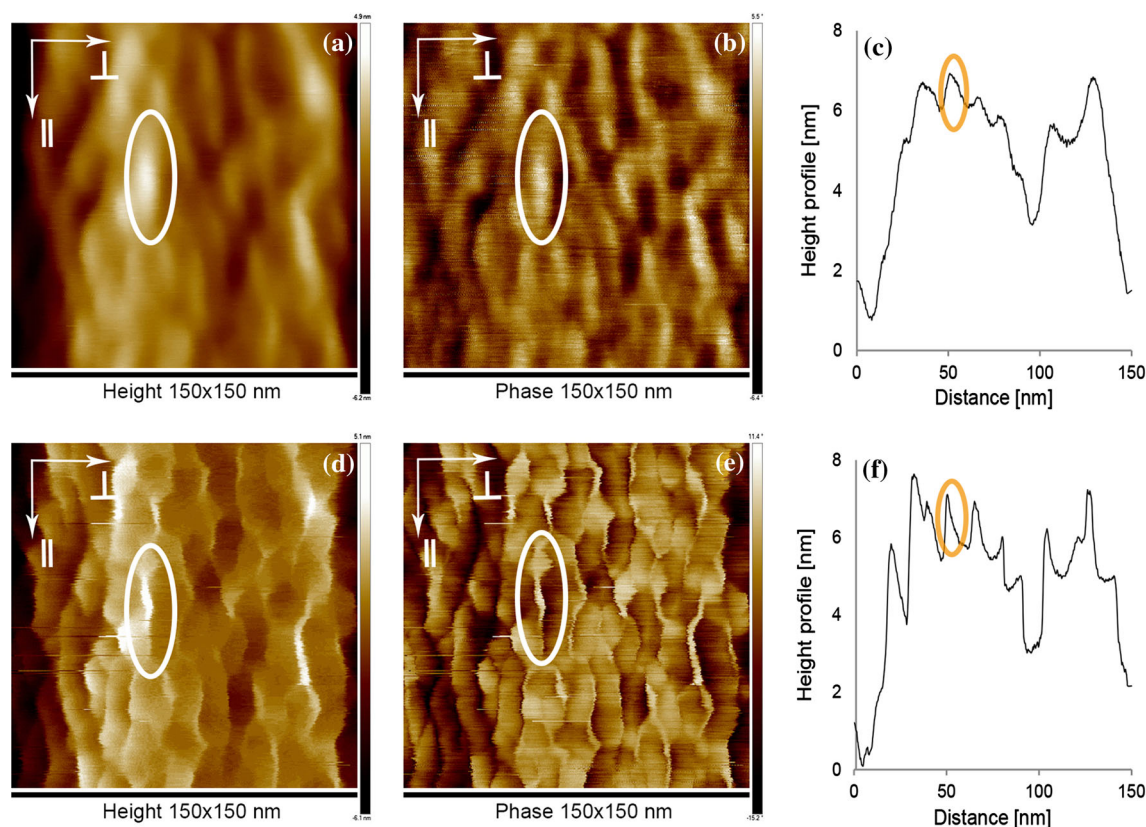

Figure 2 High-magnification AFM images of a carbon fiber surface (CF HS) scanned with TESPA probe (a, b, c) and with EBD-SSS probe (d, e, f): height images (a, d), phase images (b, e) and height profile (c, f).

size of 150 nm × 150 nm (512 × 512 pixels). The images were processed using the software Nanoscope Analysis v1.40.

Results and discussion

In the following, we describe the AFM investigations on PAN-based carbon fibers and the corresponding PAN precursor fiber. The correlation between the nanoscale surface structure of carbon fibers and their mechanical properties is also addressed.

Tip radius and resolution of AFM investigations

Figure 1a, b shows the AFM height and phase images of scan size 500 nm × 500 nm of the untreated high-tensile strength carbon fiber (CF HS) measured using a standard TESPA AFM probe. The orientation of the images parallel (‖) and perpendicular (⊥) with respect to the fiber axis in this and the following figures is marked with white arrows. The AFM images show a surface morphology of untreated carbon fibers as described in literature [37]. The fibrils are oriented parallel to the fiber axis and their widths range between 85 and 110 nm. The whole surface of the fiber shows a grain-like structure, which was demonstrated on 3 CF HS fibers and at least 4 locations on each fiber. Figure 2 shows a highly resolved image of the analyzed area of Fig. 1, as marked by a white rectangle in the image. Both, height and phase images (Fig. 2a, b) as well as a height profile (Fig. 2c) are shown. Images and height profile emphasize the grain-like morphology of the surface. Exemplary one grain is marked with an white ellipsoid in Fig. 2a, b.

Figure 3 Histograms of the width (**a**) and length (**b**) distribution of the nanopores on carbon fiber surface (CF HS) scanned with EBD-SSS probe.
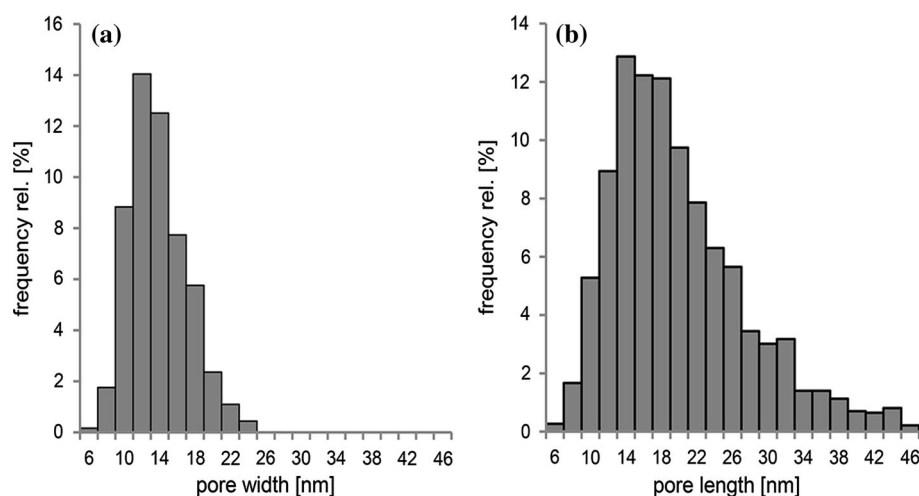

Figure 4 AFM height (**a**) and phase (**b**) image of the surface of a PAN fiber scanned with EBD-SSS probe.
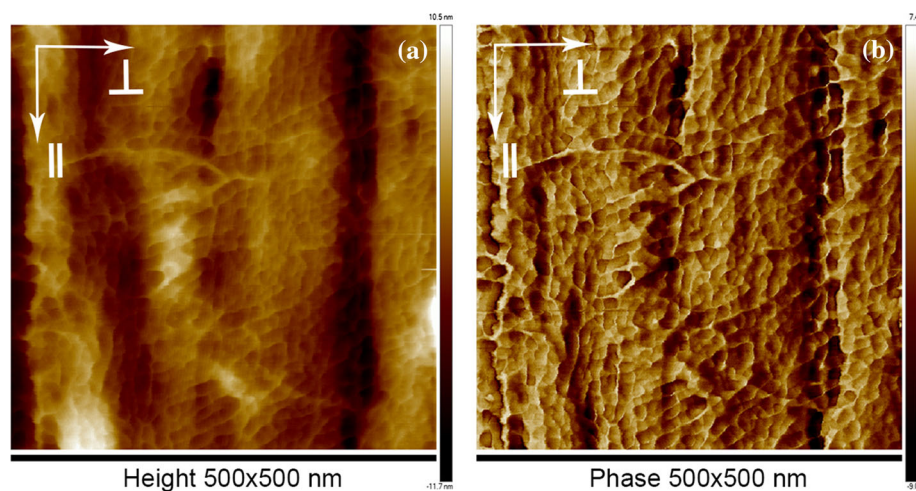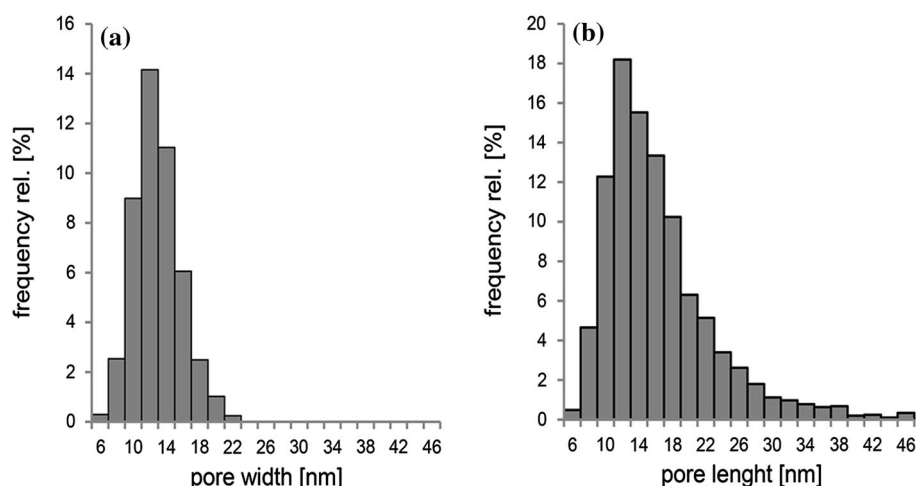
Table 1 Nanopore size of PAN fiber and carbon fiber CF HS

Fiber type	Mean width $\bar{X} \pm \sigma$ (nm)	Mean length $\bar{Y} \pm \sigma$ (nm)
PAN	11.7 ± 3.0	15.7 ± 7.7
CF HS	12.8 ± 3.1	19.3 ± 8.5

Figure 5 Histograms of the size distribution of (**a**) nanopore width and (**b**) nanopore length on PAN fiber surface measured with EBD-SSS probe.

Investigation of the carbon fibers with the extra sharp AFM tip EBD-SSS NCHR reveals new features of the surface structure. These new features are an intrinsic property of the carbon fiber, which was demonstrated by investigation of 6 fibers and more than 5 locations on each fiber. In particular, we investigated the same fiber surface region discussed above also with the sharp tip. The corresponding images are shown in Fig. 1c, d and with higher magnification in Fig. 2d, e. Instead of the grain-like structure, these new features, revealed in both height and phase images, suggest the presence of nanopores. The pores are densely arranged and homogeneously distributed over the fiber surface. In between the pores thin intersections exist, as marked in Fig. 2d, e. The pores are arranged in a chain-like structure, predominantly oriented parallel to the fiber axis. To the best of our knowledge, it is the first time that such nanopores are detected on carbon fiber surface. They seem to be the characteristic surface structure of a PAN-based carbon fiber and can only be detected by use of very sharp AFM tips.

We attribute the differences in the images taken by the two different tips to the effect, that the smaller radius of the EBD-SSS tip allows a better lateral resolution, and consequently the nanoporous structure is revealed. The dimensions of the nanopores were determined perpendicular (width) and parallel

(length) to the fiber axis by measuring the distance between two maxima in the respective direction. Evaluation of hundreds of nanopores results in a mean width of 12.8 ± 3.1 nm and a mean length of 19.3 ± 8.5 nm. The pores are separated by a thin intersection of 2–5 nm and have an average depth of 2–5 nm.

To interpret the images taken with the TESPA tip, a direct comparison of the nanostructures located at the same position (marked in Fig. 2a, b, d, and e by a white ellipsoid) is performed. The high-resolution images taken with the EBD-SSS tip (Fig. 2d, e) have to be convoluted with the tip radius of about 8 nm. This results in a broadening of the intersection, and a corresponding size reduction of the nanopores in between, and, thereby, explains the granular surface structure observed with the TESPA tip. The mean distance between the grains perpendicular to the fiber axis, as measured by the TESPA probes, is 11.5 ± 2.3 nm. The average length is 21.8 ± 6.6 nm. Both values are consistent with the nanoporous structure observed by the EBD-SSS tip. The height of the granules is 1–4 nm, which corresponds to the depth of the pores.

The resolution-dependent differences in our AFM images are demonstrated by comparison of the height profiles taken by the two different tips (see Fig. 2c, f). The ellipsoids mark one of the positions where the

Table 2 Carbon fiber types and their mechanical properties

Manufacturer	Fiber type	Tensile strength (GPa)	Tensile moduli (GPa)
Toray	T700	4.9	230
Toray	T300	3.5	230
Toray	M40	2.7	392

Figure 6 AFM images of topography and phase of the surfaces of T700 (**a**, **b**), T300 (**c**, **d**), and M40 (**e**, **f**).
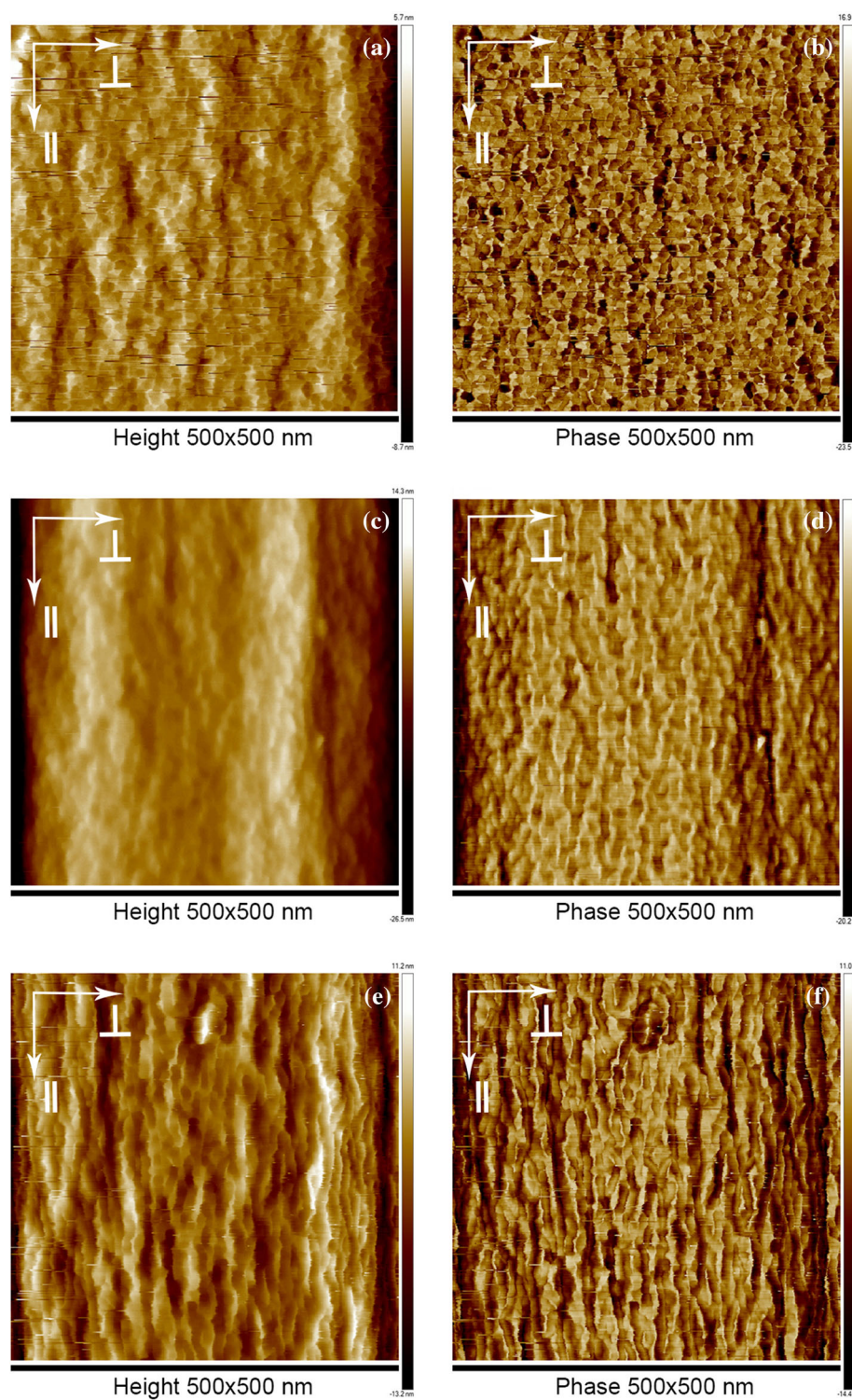
profile of a thin wall is broadened to a grain-like structure.

The histograms in Fig. 3 illustrate the frequency distributions of width and length of nanopores as measured by EBD-SSS probes. Both distributions are unimodal with the mean length approximately twice than the mean width. The fact that the lengths of the pores are larger than their widths probably results from a stretching of the initially round pores due to the stretching of the fiber during processing. The histogram of the width of the nanopores shows an almost symmetric frequency distribution. In contrast to that, the histogram of the length of the nanostructures is asymmetric with a Pearson Mode Skewness of 0.6. We also detect structures which suggest that nanopores coalesce during processing. This might explain the relatively broad length distributions of pores shown in Fig. 3b. The asymmetry results from a small number of pores with large widths. This is consistent with the observation that a minority of pores coalesce during processing.

Nanostructures on PAN fiber surface

To shed light on the origin of the observed nanoscale surface features of the carbon fiber CF HS, we turned to an early stage of the process chain, i.e., we investigated the surface of the corresponding PAN precursor fiber in an analogous manner by AFM using the sharp EBD-SSS tip. Figure 4a, b shows the height and phase images taken from the PAN fiber with scan ranges corresponding to Fig. 1. Both images show a nanoporous surface structure similar to that of the carbon fibers. In addition to the nanoporous structure, some regions of the PAN fiber surface exhibit bridge-like structures across the fibrils, oriented perpendicular to the fibril axes.

The average width and length of the pores is determined as 11.7 ± 3.0 and 15.7 ± 7.7 nm, respectively. This is in good agreement with the nanopore size on the carbon fiber surface, as summarized in Table 1. The higher values of the pore length compared to their width again can be explained by the elongation of pores during the stretching steps of the PAN fiber and a coalescing of pores, as discussed in Chap. 3.1. The latter fact is confirmed by the similar asymmetry of the length distribution curves with a Pearson Mode Skewness of 0.5 compared to the carbon fiber (see histogram in Fig. 5b). Within the margins of error, the pore width and length of PAN fibers

and carbon fibers coincide. However, a small trend to higher pore length of the carbon fiber may exist, which could be caused by the further stretching of the fibers during processing.

The presence of the porous nanostructure of the PAN fiber surface suggests that the nanopores already develop during the very beginning of the spinning process and have their origin in the fiber formation during the coagulation process of the wet spinning.

Apparently, the nanoporous structure is largely conserved along the process chain of carbon fiber production.

Carbon fiber nanostructures and mechanical properties

The mechanical properties of the carbon fibers are correlated to their structural properties [4, 48–50]. In the following, we want to investigate a possible correlation between surface structural properties and mechanical properties. To this end, the surface of carbon fibers with different tensile elastic moduli and tensile strengths have been investigated using AFM. For comparability, carbon fibers of the same manufacturer were chosen. Their mechanical properties are listed in Table 2 [45–47].

Figure 6 shows the AFM height and phase images of the carbon fibers with high tensile strength/low modulus T700 (a, b), intermediate tensile strength/ low modulus T300 (d, e), and low tensile strength/ high modulus M40 (g, h). All fibers show the nanoporous surface structure. The average size of the nanopores increases in the following order: T700, T300, and M40. The numerical values of width and length are given in Table 3. Consequently, the pore area increases. A measure of the pore area is the product of width times length which we define as effective pore area A_{eff}. The effective pore areas of the fibers T700, T300, and M40 amount to $A_{eff} = 97$, $A_{eff} = 314$, and $A_{eff} = 707$, respectively. Also, we

Table 3 Nanopores on the surface of different carbon fibers

Fiber type	Mean width $\bar{X} \pm \sigma$(nm)	Mean length $\bar{Y} \pm \sigma$(nm)
T700	9.7 ± 2.0	10.0 ± 2.7
T300	11.6 ± 2.2	27.1 ± 14.1
M40	14.2 ± 3.1	50.5 ± 25.0
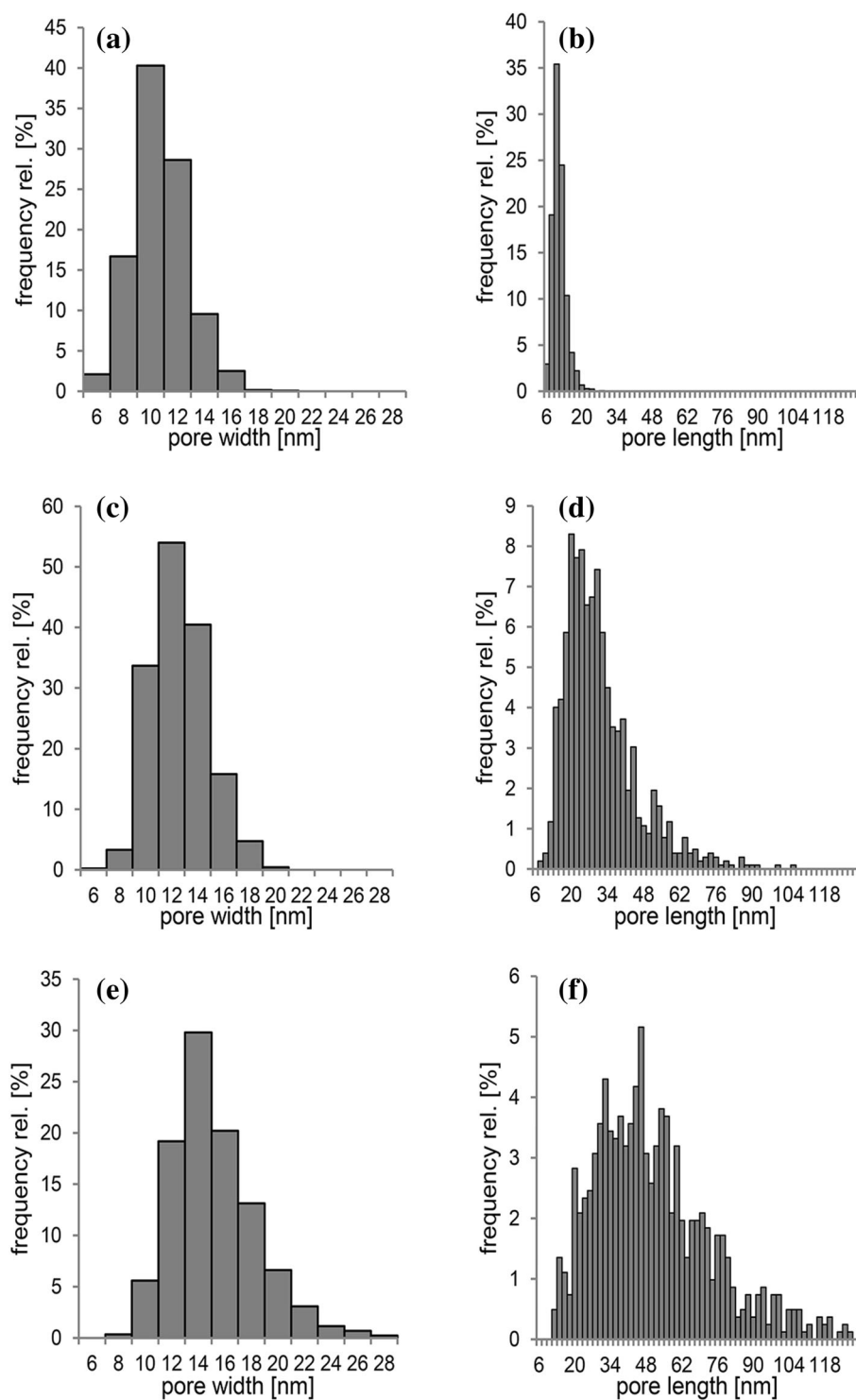
Figure 7 The histograms (**a**, **c**, **e**) show the distribution of the pore width, the histograms (**b**, **d**, **f**) show the distribution of the pore length of T700, T300, and M40.

observe significant differences in the shape of the nanopores of the different fibers, in particular in the aspect ratio ($a = $ length/width). The nanopores of

T700 have an almost round shape with an aspect ratio of 1.0, and are individually enclosed by the fiber matrix. In contrast to that, the aspect ratio of
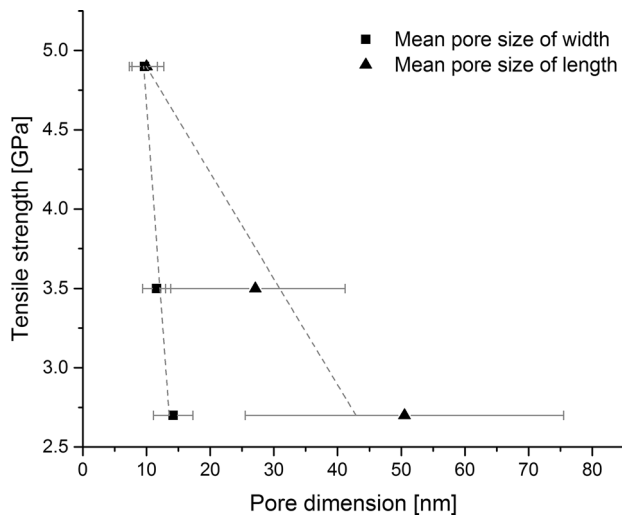
Figure 8 Correlation between tensile strength and pore dimensions.

Table 4 Roughness analysis values

Fiber type	Mean nanoroughness $\bar{R}_a \pm \sigma$ (nm)
T700	0.8 ± 0.0
T300	1.4 ± 0.2
M40	1.8 ± 0.2
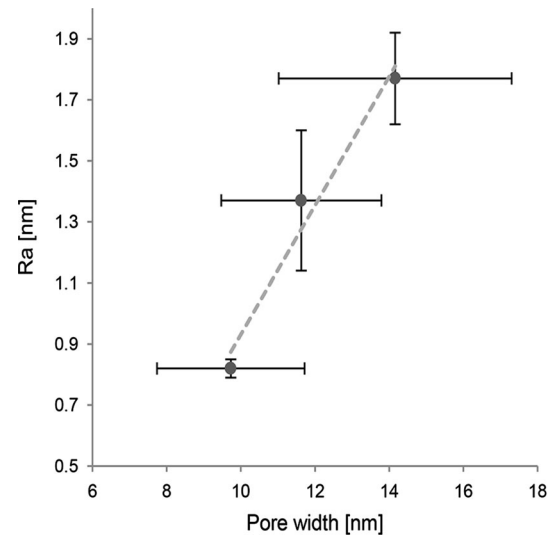
Figure 9 Pore width as function of roughness R_a.

the nanopores of fibers T300 and M40 is significantly higher with $a = 2.3$ and $a = 3.6$, respectively. For the latter two fibers, the pores apparently have coalesced and formed channels. This observation is distinct for fiber M40, but only faintly visible for fiber T300. Again the effect that a certain number of pores have coalesced is expressed by the asymmetry of the distribution curve of the pore length (see Fig. 7b, d, f).

Comparison of the effective pore area with the mechanical properties of the three different carbon fibers reveals a clear correlation, as demonstrated in the correlation plot in Fig. 8. It shows that the tensile strength of the carbon fibers decreases with increasing pore widths and pore lengths. This effect is more distinct for the pore length. This decreasing tensile strength with increasing effective pore area might be due to a notch effect caused by the pores on the fiber surface [51]. Another explanation might be that the surface defect structure is a measure of the bulk defect structure, i.e., larger defects on the surface point to larger defects in the bulk of the respective fibers, resulting in a decrease of the tensile strength.

It can be expected that the nanopore density of the fiber surface is reflected by its surface roughness [52–55]. The surface roughness of the carbon fibers is calculated from the AFM data using a suitable background correction. For the evaluation of the nanoscale surface roughness (nanoroughness), we use the method of Jäger et al. with a symmetric baseline and

$\eta = 5 \times 10^2$ [56]. The nanoroughness values R_a are summarized in Table 4. As shown in Fig. 9, the surface roughness increases with increasing pore width. Consequently, the tensile strength of the carbon fiber decreases with increasing nanoroughness.

Conclusion

We have investigated the surface of PAN-based carbon fibers by AFM utilizing two different AFM probes, a standard tip and a super sharp tip. Using the super sharp AFM tip with small tip radius, a so far not resolved nanoporous surface structure has been revealed. The nanopores are distributed homogeneously over the surface of the carbon fibers. Nanopores with a similar diameter are also detected on the surface of corresponding PAN fibers. This suggests that nanopores are maintained along the process chain of stabilization and carbonization.

The mechanical properties of the carbon fibers appear to be correlated to the size and the shape of the nanopores. The tensile strength decreases with increasing effective pore area and pore aspect ratio.

The variation of the average pore size is well reflected by the nanoroughness of the respective fiber.

Further investigations should address the correlation between surface and volume structure on a nanoscale.

Compliance with ethical standards

Conflicts of interest The authors declare that they have no conflict of interest.

References

[1] Frank E, Steudle LM, Ingildeev D, Spörl JM, Buchmeiser MR (2014) Carbon fibers: precursor systems, processing, structure, and properties. Angew Chem Int Ed 53(21):5262–5298

[2] Chand S (2000) Review: carbon fibers for composites. J Mater Sci 35(6):1303–1313. doi:10.1023/A:1004780301489

[3] Huang X (2009) Fabrication and properties of carbon fibers. Materials 2(4):2369–2403

[4] Fitzer E (1989) Pan-based carbon fibers—present state and trend of the technology from the viewpoint of possibilities and limits to influence and to control the fiber properties by the process parameters. Carbon 27(5):621–645

[5] Mark HF (2007) Encyclopedia of polymer science and technology, 3rd edn. Wiley-Interscience, Hoboken

[6] Morita K, Murata Y, Ishitani A, Murayama K, Ono T, Nakajima A (1986) Characterization of commercially available PAN (polyacrylonitri1e)-based carbon fibers. Pure Appl Chem 58(3):455–468

[7] Damodaran S, Desai P, Abhiraman AS (2008) Chemical and physical aspects of the formation of carbon fibres from PAN-based precursors. J Text Inst 81(4):384–420

[8] Paul DR (1968) A study of spinnability in the wet-spinning of acrylic fibers. J Appl Polym Sci 12(10):2273–2298

[9] Cahn JW (1965) Phase separation by spinodal decomposition in isotropic systems. J Chem Phys 42(1):93

[10] Cohen C, Tanny GB, Prager S (1979) Diffusion-controlled formation of porous structures in ternary polymer systems. J Polym Sci Polym Phys 17(3):477–489

[11] Arbab S, Noorpanah P, Mohammadi N, Soleimani M (2008) Designing index of void structure and tensile properties in wet-spun polyacrylonitrile (PAN) fiber. I. Effect of dope polymer or nonsolvent concentration. J Appl Polym Sci 109(6):3461–3469

[12] Weisser P, Barbier G, Richard C, Drean J (2015) Characterization of the coagulation process: wet-spinning tool development and void fraction evaluation. Text Res J. doi:10.1177/0040517515606355

[13] Baojun Q, Ding P, Zhenqiou W (1986) The mechanism and characterstics of dry-jet wet-spinning of acrylic fibers. Adv Polym Technol 6(4):509–529

[14] van de Witte P, Dijkstra PJ, van den Berg J, Feijen J (1996) Phase separation processes in polymer solutions in relation to membrane formation. J Membr Sci 117(1–2):1–31

[15] Knudsen JP (1963) The influence of coagulation variables on the structure and physical properties of an acrylic fiber. Text Res J 33(1):13–20

[16] Gupta AK, Paliwal DK, Bajaj P (1991) Acrylic precursors for carbon fibers. Polym Revs 31(1):1–89

[17] Bajaj P, Munuktla Surya Kumari, Vaidya AA, Gupta DC (1989) Influence of spinning dope additives and spin bath temperature on the structure and physical properties of acrylic fibers. Text Res J 59(10):601–608

[18] Fitzer E, Frohs W (1990) Modern carbon fibres from polyacrylonitrile (PAN)-polyheteroaromatics with preferred orientation. Chem Eng Technol 13(1):41–49

[19] Wilms C, Seide GH, Gries T (2013) The relationship between process technology, structure development and fibre properties in modern carbon fibre production. Chem Eng Trans 32:1609–1614

[20] Dilsiz N, Wightman J (1999) Surface analysis of unsized and sized carbon fibers. Carbon 37(7):1105–1114

[21] Song W, Gu A, Liang G, Yuan L (2011) Effect of the surface roughness on interfacial properties of carbon fibers reinforced epoxy resin composites. Appl Surf Sci 257(9):4069–4074

[22] Johnson DJ, Tyson CN (1969) The fine structure of graphitized fibres. J Phys D Appl Phys 2(6):787–795

[23] Bashir Z (1994) Co-crystallization of solvents with polymers: the x-ray diffraction behavior of solvent-containing and solvent-free polyacrylonitrile. J Polym Sci Polym Phys 32(6):1115–1128

[24] Warner SB, Uhlmann DR (1979) Oxidative stablzation of acrylic fibres. J Mater Sci 14(8):1893–1900. doi:10.1007/BF00553962

[25] Badami DV, Joiner JC, Jones GA (1967) Microstructure of high strength, high modulus carbon fibres. Nature 215(5099):386–387

[26] Bennett SC, Johnson DJ (1979) Electron-microscope studies of structural heterogeneity in pan-based carbon fibres. Carbon 17(1):25–39

[27] Johnson DJ, Frank C (1980) Recent Advances in Studies of Carbon Fibre Structure [and Discussion]. Philos Trans R Soc A Math Phys Eng Sci 294(1411):443–449

[28] Johnson DJ (1987) Structure-property relationships in carbon fibres. J Phys D Appl Phys 20(3):286–291

[29] Brasquet C, Rousseau B, Estrade-Szwarckopf H, Le Cloirec P (2000) Observation of activated carbon fibres with SEM

and AFM correlation with adsorption data in aqueous solution. Carbon 38(3):407–422

[30] Qian X, Zou R, OuYang Q, Wang X, Zhang Y (2015) Surface structural evolvement in the conversion of polyacrylonitrile precursors to carbon fibers. Appl Surf Sci 327:246–252

[31] Yao L, Li M, Wu Q, Dai Z, Gu Y, Li Y, Zhang Z (2012) Comparison of sizing effect of T700 grade carbon fiber on interfacial properties of fiber/BMI and fiber/epoxy. Appl Surf Sci 263:326–333

[32] Donnet JB, Qin RY (1993) Study of carbon fiber surfaces by scanning tunneling microscopy, Part II-PAN-based high strength carbon fibers. Carbon 31(1):7–12

[33] Shi D, Liu N, Yang H, Gao J, Jiang Y, Pang S, Wu X, Ji Z (1997) Scanning tunneling microscope study of polyacrylonitrile-based carbon fibers. J Mater Res 12(10):2543–2547

[34] Yoon S, Korai Y, Mochia I, Yokogawa K, Fukuyama S, Yoshimura M (1996) Axial nano-scale microstructures in graphitized fibers inherited from liquid crystal mesophase pitch. Carbon 34(1):83–88

[35] Magonov SN (1993) Surface characterization of materials at ambient conditions by scanning tunneling microscopy (STM) and atomic force microscopy (AFM). Appl Spec Rev 28(1–2):1–121

[36] Li W, Long D, Miyawaki J, Qiao W, Ling L, Mochida I, Yoon S (2012) Structural features of polyacrylonitrile-based carbon fibers. J Mater Sci 47(2):919–928. doi:10.4236/aces.2012.22032

[37] Magonov SN, Bar G, Cantow H, Bauer H, Muueller I, Schwoerer M (1991) Atomic force microscopy on polymers and polymer related compounds. Polym Bull 26(2):223–230

[38] Binnig G, Gerber C, Stoll E, Albrecht TR, Quate CF (1987) Atomic resolution with atomic force microscope. Europhys Lett 3(12):1281–1286

[39] Zhong Q, Inniss D, Kjoller K, Elings VB (1993) Fractured polymer/silica fiber surface studied by tapping mode atomic force microscopy. Surf Sci Lett 290(1–2):L688–L692

[40] Paulo ÁS, García R (2002) Unifying theory of tapping-mode atomic-force microscopy. Phys Rev B 66(4):041406

[41] Keller DJ, Chih-Chung C (1992) Imaging steep, high structures by scanning force microscopy with electron beam deposited tips. Surf Sci 268(1–3):333–339

[42] Bustamante C, Keller D, Yang G (1993) Scanning force microscopy of nucleic acids and nucleoprotein assemblies. Curr Opin Struc Biol 3(3):363–372

[43] Engel A, Schoenenberger C, Müller DJ (1997) High resolution imaging of native biological sample surfaces using scanning probe microscopy. Curr Opin Struc Biol 7(2):279–284

[44] Shao Z, Mou J, Czajkowsky DM, Yang J, Yuan J (1996) Biological atomic force microscopy: what is achieved and what is needed. Adv Phys 45(1):1–86

[45] Toray (T300) Product literature

[46] Toray (T700) Product literature

[47] Toray (M40) Product literature

[48] Cooper GA, Mayer RM (1971) The strength of carbon fibres. J Mater Sci 6(1):60–67. doi: 10.1007/BF00550292

[49] Edie DD (1998) The effect of processing on the structure and properties of carbon fibers. Carbon 36(4):345–362

[50] Liu F, Wang H, Xue L, Fan L, Zhu Z (2008) Effect of microstructure on the mechanical properties of PAN-based carbon fibers during high-temperature graphitization. J Mater Sci 43(12):4316–4322. doi: 10.1007/s10853-008-2633-y

[51] Johnson JW, Thorne DJ (1969) Effect of internal polymer flaws on strength of carbon fibres prepared from an acrylic precursor. Carbon 7(6):659–661.

[52] Khulbe KC, Feng CY, Matsuura T (2008) Synthetic polymeric membranes. Springer, Berlin

[53] Bowen W, Hilal N, Lovitt RW, Williams PM (1996) Atomic force microscope studies of membranes: surface pore structures of Diaflo ultrafiltration membranes. J Colloid Interf Sci 180(2):350–359

[54] Sun J, Hu Y, Frieze WE, Chen W, Gidley DW (2003) How pore size and surface roughness affect diffusion barrier continuity on porous low-k films. J Electrochem Soc 150(5):F97

[55] Souhaimi MK, Matsuura T (2011) Membrane distillation: principles and applications, 1st edn. Elsevier professional, Boston

[56] Jäger J, Moosburger-Will J, Horn S (2013) Determination of nano-roughness of carbon fibers by atomic force microscopy. J Mater Sci 48(19):6803–6810. doi:10.1007/s10853-013-7485-4